

Subgrid Combustion Modeling for Premixed Turbulent Reacting Flows *

Thomas M. Smith [†] and Suresh Menon [‡]
 School of Aerospace Engineering
 Georgia Institute of Technology
 Atlanta, Georgia 30332-0150
 email: *menon@falcon.ae.gatech.edu*

Abstract

Two combustion models for turbulent premixed combustion in the flamelet regime are developed for unsteady simulations. The first model is a conventional G equation flamelet model and the main issues discussed are the subgrid closure. The second model is based on the Linear-Eddy Model. Both models are used in simulation of turbulent stagnation point flames. The heat release and turbulence intensity are varied. Time averaged statistics from conventional simulations show good qualitative agreement with experiments and the normalized turbulent flame speed agrees well with the experimental data. Counter-gradient scalar diffusion is observed in high heat release, low turbulence intensity flames. This raises the question about how important the gradient diffusion approximation is to these results. Preliminary results from LES-LEM simulations involving moderate heat release and high turbulence intensities are reported. The key role of the front tracking algorithm is demonstrated. Qualitative trends in the burning rates with varying turbulence intensity is also demonstrated.

1 Introduction

Of central importance to the understanding and prediction of turbulent flame propagation physics are flame/turbulence responses to varying laminar flame speeds (S_L), turbulence intensities (u'), and turbulence length scales (l). While S_L may be assumed constant in many flows (flamelet approximation), turbulence velocity and length scales vary greatly and so flamelet response to a changing hydrodynamic field is a local phe-

nomena. In addition, alteration of the hydrodynamic field, mainly due to dilatation and increased viscous effects occur simultaneously. For these reasons, steady state approaches for predicting flame/turbulence interactions are limited. The problem may be solved, in theory, by direct numerical simulation (DNS). However, DNS is highly restricted to a narrow band of length and time scales due to available computational resource limitations.

Large-Eddy simulation (LES) is an emerging technology that bridges the gap between (DNS) and the Reynolds Averaged Navier-Stokes (RANS) approach. The concept of LES is based on physical arguments about resolved and unresolved (subgrid) scales existing in the flow. These physical arguments are summarized by Ferziger (1983): 1) The largest eddies interact with the mean flow while the small eddies are created by nonlinear interactions among the large eddies. 2) The structure of large scales is strongly dependent on geometry and are therefore anisotropic (usually vortical) while the small scales are more isotropic and universal. 3) Large eddy time scales approximate the time scales of the mean flow while subgrid time scales are much shorter since small eddies are created and destroyed more rapidly than large scales. 4) Most of the transport of mass, momentum, energy, and concentrations is due to the large scales while small scales mainly dissipate fluctuations in these quantities.

The consequences of these arguments are: 1) Large scales are much harder to model and it is unlikely that a universal model may be found. On the other hand, small scales are much easier to model due to their universal character and a model for small scales is more likely to be found. 2) Most of the transport is computed directly. 3) The computational cost increases compared to RANS. This leads to the concept of large-eddy simulation where the large scales are directly computed and the effect of the small scales on the large scales is modeled.

*Copyright ©1998 by T. M. Smith and S. Menon. Published by the American Institute of Aeronautics and Astronautics, Inc., with permission.

[†]Graduate Research Assistant, Student Member, AIAA

[‡]Professor, Senior Member, AIAA

Subgrid combustion modeling differs from subgrid turbulence modeling in that usual assumptions made for momentum and energy equation closures are suspect for reacting scalars. Namely, the gradient diffusion assumption (Boisseries approximation, where an apparent viscosity called the eddy viscosity and the mean stress tensor are combined to model the Reynolds stress tensor) may be valid for momentum and energy so that relatively simple models may be used. However, in the case of diffusive-reactive scalars, combustion is dominated by mixing processes and premixed flamelet propagation rates are greatly influenced by micro-scale wrinkling. Micro-scale mixing and flame surface wrinkling are not adequately modeled by gradient diffusion. In addition, counter-gradient diffusion has been observed in reacting flows having significant heat release.

In an earlier paper (Smith and Menon, 1997) the computational methodology for simulating stagnation point flames was demonstrated. In that study, the flame propagation was described using an uncoupled LES-LEM approach. This paper continues the development of the stagnation point flame simulations using both the conventional flamelet model and the LES-LEM method of computing turbulent reacting flows. Some important features of the LES-LEM methodology include; appropriate characterization of unresolved fine-scale wrinkling and flamelet burning, the resolved scale transport of the progress variable by the resolved scale turbulence and thermodynamic coupling between the subgrid and the resolved field.

Stagnation point flames have several advantages that are exploited in order to evaluate this modeling approach. First, the flow is stationary and, thus, the flame position and propagation rate are steady. The steady nature of these flows allows for statistical properties to be analyzed. Since the subgrid model is stochastic, precise evolution of the burning surface is not available. Instead a stationary turbulent flame structure is computed that is suitable for comparison with existing experimental data. Secondly, the turbulence intensity and heat release can be parameterized to test how the subgrid combustion model and the resolved scale progress variable respond to these hydrodynamic inputs.

2 Model Formulation

The LES-LEM modeling approach is described in this section. The model consists of the conventional LES framework, the subgrid combustion model and the coupling mechanism that links subgrid combustion to the LES resolved field solution and resolved field convection to the transport of LEM cells.

2.1 Large-Eddy Simulation

The equations of LES are the mass weighted spatially filtered mass, momentum, energy, and species equations. Subgrid terms are a result of filtering nonlinear terms in the equations and models must be found for them. Of particular interest is the filtered species equation which contains a subgrid flux that is due to the unresolved turbulent velocity field and the mean reaction rate. Both of these unknown terms are troublesome. The subgrid flux $\bar{\rho}[u_i \bar{Y}_k - \tilde{u}_i \bar{Y}_k]$ is the transport of species mass fraction by subgrid scale turbulence and is responsible for micro-scale mixing. The mean reaction rate $\bar{\omega}_k$ depends on correlations between resolved and unresolved temperature (\bar{T}, T''), and between resolved and unresolved species (\bar{Y}_k, Y_k'') correlations and is very difficult to evaluate. A common practice is to evaluate the probability density function (pdf) of the reaction rate as a function of resolved variables. Though a closed form expression for $\bar{\omega}_k$ can be found, these methods are mainly used for steady state calculations and modeling micro-scale mixing is not straight forward.

The current approaches replace the filtered species equations with a conventional flamelet model referred to as the G equation and a subgrid combustion model where the scalars evolve according to diffusion-reaction equations and stochastic rearrangement events representing turbulent stirring.

2.2 G -Equation Flamelet Model

The flamelet assumption describes a regime in premixed combustion that is often encountered in practical combustion devices. Within the flamelet assumption, the flame thickness (δ_f) is small compared to the smallest dynamic scale (η , the Kolmogorov scale) of turbulence and the characteristic burning time (τ_c) is small compared to the characteristic flow time (τ). As a result, the flame structure remains unaltered and the flame can be considered a thin front propagating at a speed dictated by the mixture properties that is wrinkled and convected by the flow. A model equation that describes the propagation of a thin flame by convective transport and normal burning (self propagation by Huygens' principle) has been introduced called the G -field equation (Williams, 1985; Kerstein *et al.*, 1988)

$$\frac{\partial G}{\partial t} + \mathbf{u} \cdot \nabla G = S_L |\nabla G| \quad (1)$$

where G is a progress variable that defines the location of the flame, \mathbf{u} is the mass averaged velocity vector and S_L is the local laminar flame speed. Equation (1) describes the convection of a level surface, defined as $G = G_o$, by the fluid velocity while simultaneously undergoing propagation normal to itself at a speed S_L

according to Huygens' principle. In the flow field, the value of G is in the range $[0,1]$ and in flame front modeling, G exhibits a step function like behavior, separating the burnt region ($G < G_o$) from the unburned region ($G > G_o$). G is assigned the value of unity in the unburned region and zero in the burnt region with the thin flame identified by a fixed value of $0 < G_o < 1$. In the finite-volume numerical approach, an equivalent equation is written

$$\frac{\partial \rho G}{\partial t} + \nabla \cdot \rho \mathbf{u} G = \rho_o S_L^o |\nabla G| \quad (2)$$

where ρ_o is the reference reactant density and S_L^o is the undisturbed laminar flame speed. The relationship, $\rho_o S_L^o = \rho S_L$ is an expression of mass conservation through the flame.

Upon filtering

$$\frac{\partial \bar{\rho} \tilde{G}}{\partial t} + \nabla \cdot \bar{\rho} \tilde{\mathbf{u}} \tilde{G} = \overline{\rho_o S_L^o |\nabla G|} - \nabla \cdot (\bar{\rho} [\tilde{\mathbf{u}} \tilde{G} - \tilde{\mathbf{u}} \tilde{G}]). \quad (3)$$

The unresolved transport term is modeled using a gradient assumption (Im, 1995; Im *et al.*, 1997 and Piana *et al.*, 1997)

$$\bar{\rho} [\tilde{\mathbf{u}} \tilde{G} - \tilde{\mathbf{u}} \tilde{G}] \approx -\frac{\mu_t}{Sc^G} \nabla \tilde{G} \quad (4)$$

where μ_t is an eddy viscosity and Sc^G is a Schmidt number. At first glance, the gradient closure approximation appears to clearly violate the physics of turbulent transport given that counter-gradient diffusion dominates the transport of scalar fluxes in many situations. However, it must be kept in mind that counter-gradient transport is a large scale phenomena (Bray, 1995) and in the LES methodology, the large scales are directly computed and therefore, counter-gradient diffusion should be accounted for despite the subgrid closure assumed. This, of course, will require evaluation. In addition, counter-gradient diffusion is produced by the preferential acceleration of lighter parcels of fluid as opposed to heavier parcels by the mean pressure gradient. Given the current subgrid modeling technology, pressure gradient effects are not included in the closure models and therefore the ability to produce counter-gradient diffusion is absent from all models that neglect pressure effects.

For closure of the source term, Yakhot's RNG model is used (Yakhot, 1988; Menon and Jou, 1991). This model is an analytical expression for the turbulent flame speed as a function of turbulence intensity ($u_t/S_L = \exp[u'^2/u_t'^2]$) obtained from Eq. (1). For flamelet combustion, $\frac{A_t}{A_l} = \frac{u_t}{S_L}$ where A_t and A_l are the turbulent and laminar flame areas respectively, and therefore Yakhot's model is an estimate of the flame wrinkling due to the turbulence intensity. Therefore, in the LES

context, the propagation rate is no longer $\rho_o S_L^o$ but is instead replaced by $\rho_o u_f$ where u_f is obtained from ($u_f/S_L = \exp[(u'_{sgs})^2/(u_f)^2]$) which is the subgrid turbulent burning rate that accounts for unresolved flame wrinkling. The turbulence intensity appearing in the turbulent flame speed model is the subgrid turbulence intensity, $u'_{sgs} = \sqrt{\frac{2}{3} k^{sgs}}$ where k^{sgs} is the subgrid turbulent kinetic energy given by, $k^{sgs} = \frac{1}{2} [\overline{u_l u_l} - \tilde{u}_l \tilde{u}_l]$. Note that $u'_{sgs} \neq u_i''$ which represents the fluctuating part of u_i . A model equation for the subgrid turbulent kinetic energy is discussed in Smith and Menon (1997). It was argued there that in two-dimensional constant flame speed simulations, the subgrid kinetic energy is negligible and therefore, subgrid closure terms can be neglected. In the present study, the subgrid terms are included and the subgrid turbulence intensity is retained to provide a measure of the subgrid flame speed through Yakhot's model.

This model assumes that the flame is a thin sheet having no internal structure and, therefore, is applicable only in the flamelet combustion regime. Furthermore, it does not take into account flame stretching effects and so cannot predict extinction. However, it has been shown that the model compares well with experimental data in the low to moderately high u'/S_L range and also predicts (in reasonable agreement with data) a rapid increase in u_t/S_L at low u'/S_L and then a *bending* slope at high u'/S_L (Yakhot, 1988). The source term for the filtered G equation becomes

$$\overline{\rho_o S_L^o |\nabla G|} \approx \rho_o u_t |\nabla \tilde{G}|. \quad (5)$$

Thermodynamic coupling is through the internal energy $\tilde{e} = c_v \tilde{T} + \Delta h_f \tilde{G}$, where $\Delta h_f = c_p (T_p - T_f)$ is the heat of formation, c_v and c_p are the specific heats at constant volume and pressure respectively. In cases of non-zero heat release, the internal energy is now a function of G , $\tilde{e} = c_v \tilde{T} + h_f G$ where $h_f = c_p (T_p - T_f)$ is a heat release parameter. In this case h_f should be a heavy side function of G , however, this produces a numerical instability when the flame front is steeply varying. Menon (1991) has pointed out that the linear dependence on G results in a distributed heat release that tracks the flame and does not cause significant error as long as the front is not a broad front.

2.3 Linear-Eddy Model

The linear-eddy model of Kerstien (1991) was originally developed as a mixing model for diffusive scalars. It was later shown capable of predicting turbulent combustion processes in flows having a large degree of symmetry. In recent years it has been adapted to LES as a subgrid combustion model for turbulent diffusion

flames (Calhoun and Menon 1996; 1997). It has also been shown capable of characterizing premixed turbulent flame propagation in isotropic flows (Smith and Menon; 1996a, 1996b). In this paper, the LEM is adopted as a subgrid model for premixed flame propagation in the laminar flamelet regime.

The LEM model can be described as a direct simulation of diffusive-reactive scalars in isotropic turbulence on a linear domain. A system of reaction-diffusion equations that describe the continuous evolution of scalars (not containing an explicit velocity) on a line are subjected to instantaneous rearrangement events each one mimicking the action of a single eddy. For flamelet regime combustion ($\delta_l \ll \eta$), using the G -field equation, a model for flamelet combustion using the linear-eddy approach is formulated (designated GLEM). GLEM models laminar burning by the propagation equation (Menon and Kerstein, 1992; Smith and Menon, 1996b)

$$\frac{\partial G}{\partial t} = S_L |\nabla G|. \quad (6)$$

This equation tracks the propagation of a single value of G between $G_{fuel} \leq G_o \leq G_{prod}$, where $G_{fuel} = 1$ and $G_{prod} = 0$. G_o is a pre specified level surface representing the location of the flame. Therefore, flame propagation is described by one scalar instead of $N + 1$ (Menon and Kerstein, 1992). The flame speed S_L is also a pre specified constant which accounts for all of the physio-chemical properties of the mixture. Since LEM resolves even step-like fronts, no dissipation mechanism is necessary to prevent false minima from occurring.

Stochastic rearrangements of scalar fields is accomplished by the triplet map, Kerstein (1991). The rearrangement events are governed by three parameters; location of mapping event, size of the event and the frequency per unit length of events. The parameters are obtained by equating the total diffusivity of a random walk of a marker particle with the turbulent diffusivity ($u'l$) in inertial range turbulence. This stirring process wrinkles the subgrid G field increasing the per LES cell burning rate, which is estimated as the number of flame crossings (G_o) in the LES cell. For a more detailed description see Smith and Menon (1997).

2.4 Linear-Eddy Subgrid Combustion Model

The remaining component in the LES-LEM formulation is the coupling between the subgrid combustion and the resolved scale flow quantities. LES-LEM coupling is accomplished by resolved scale convection and by specifying the subgrid Re and length scale.

Large scale convection between two adjacent LES cells is handled by *splicing* subgrid cells from a donat-

ing LES cell to a receiving LES cell (Menon *et al.*, 1994; Calhoun and Menon, 1996). The splicing algorithm (i) calculates the volume flux to be transferred across the LES cell interface (in a finite volume formulation) based on the resolved velocity and subgrid turbulence intensity ($\tilde{u}_i + u'_{sgs}$), (ii) removes an equivalent number of LEM cells from the donor LES cell, and, (iii) adds them to the receiving LES cell. The rate of transfer is based on the convective time scale of the resolved velocity, $\Delta t_{CON} = \min\{\Delta x_{LES}/(\tilde{u}_i + u'_{sgs})\}$, (Calhoun and Menon, 1996). Spurious scalar diffusion can occur when a group of LEM cells are spliced from one cell and placed adjacent to cells in another LES cell. This is because the scalar may not be continuous at the interface. Calhoun advocated the use of subgrid partitions to help eliminate this problem. In the present study, a new approach is taken. Since spliced cells take the value of 0 or 1, upon insertion into the receiving LES cell, the new cells can be placed adjacent to cells having the same value as the cell on the end of the segment. Thus, no artificial flamelet is created by splicing. This eliminates spurious diffusion altogether. In addition, convecting scalar values of either 0 or 1 was found to greatly reduce spurious diffusion when the mean flow is not aligned with a grid direction. This issue becomes less important as Re_{sgs} increases. Re_{sgs} is obtained directly from $u'_{sgs} = \sqrt{\frac{2}{3}k^{sgs}}$ (not to be confused with u' or u'').

Two different methods of thermodynamic coupling are currently under investigation for LES-LEM. The first method is described in Calhoun and Menon (1996). In this method LEM-LES thermodynamic coupling relates the progress of the flame in each LES cell to the resolved internal energy, $\tilde{e} = c_v \tilde{T} + \Delta h_f \tilde{G}$, where \tilde{G} is the Favre filtered G that is obtained from the subgrid scalar field, $\Delta h_f = c_p(T_{prod} - T_{fuel})$ is the heat of formation, c_v and c_p are the specific heats at constant volume and pressure respectively. The second method replaces the heat of formation contained in the total energy with a source term. The source term can be calculated exactly from the unfiltered subgrid field as

$$\Delta h_f \rho_o S_L |\nabla G| = \frac{\Delta h_f \rho_o S_L \sum_{is=2}^{ISGS} |G_{is} - G_{is-1}|}{ISGS \Delta x_{LEM}}. \quad (7)$$

where $ISGS$ is the subgrid resolution and Δx_{LEM} is the subgrid cell spacing.

3 Simulation of Stagnation Point Flames

The numerical simulations of stagnation point flames were designed to mimic the experiments of Cho *et al.*

(1986), Cho *et al.* (1988), and Liu and Lenze (1988) while reducing the complexity by simplifying inflow and wall boundary conditions. A schematic diagram of the computational domain is presented in Fig. 1. A buffer region (that numerically suppresses unsteady physical fluctuations by stretching the computational grid spacing) surrounds the core grid mesh on three sides of the two-dimensional domain. A jet of diameter D (0.05m) of premixed reactants is placed $2D$ away from a flat wall. The computational domain is tilted 90 degrees to that of the experimental apparatus so the flow is from left to right, the wall is along the vertical direction and the outflow boundaries are normal to the y direction.

In the experiments, a co-flowing laminar jet surrounds the turbulent jet in order to prevent large scale entrainment from the ambient air. The computational co-flowing jet extends to the edge of the outflow boundary to prevent entrainment at the inflow, a situation that is very difficult to handle because the boundary conditions are not easily specified.

Turbulence is generated by passing the premixed stream through a grid or a plate with holes, just prior to the converging nozzle. This produces a nearly uniform homogeneous turbulent stream. Synthesized turbulence which is nearly isotropic, divergence free, and non-periodic is generated from a specified turbulent kinetic energy spectrum and turbulence intensity in a manner similar to Lee *et al.* (1992). The synthesized turbulence is convected at the local mean axial velocity and is included using forcing functions in the governing momentum equations.

The width of the domain extends $2D$ parallel to the wall. The inflow boundary is at $6D$ ahead of the jet exit and are partially reflecting. The outflow boundaries are $5D$ away from the stagnation point and are non-reflecting (Smith and Menon, 1997). A slip condition was imposed at the wall. This means that there was no boundary layer created as the flow passed over and parallel to the wall. It has been discussed in Cho *et al.* (1988) that the flame location is well outside of the thermal layer and they argue that it has no significant effect on the flame propagation. In addition, there is no significant boundary layer at the stagnation point because the transverse component of velocity is zero on the stagnation stream line. This argument is implicit in these simulations for it greatly reduces the computational cost by not requiring a refined mesh normal to the wall. Partially-reflecting characteristic based inflow boundary conditions were used (Smith and Menon, 1997). This set of boundary conditions greatly reduce the amplitude of the reflected pressure waves while allowing for the specification of an unsteady velocity inflow field. Non-reflecting characteristic boundary conditions are imposed on the vertical outflow boundaries

similar to those suggested by Poinso and Lele (1992). The wall is assumed to be slip and adiabatic.

The governing equations with boundary conditions and associated subgrid models are solved using an explicit time marching MacCormack type finite-volume scheme that is formally second-order accurate in time and fourth-order accurate in space (Nelson and Menon, 1998). In the buffer regions of the domain, the order of the scheme has been reduced to second-order in space (which is known to be significantly more dissipative than fourth-order) in order to provide additional damping of oscillations. The code has been implemented with the MPI message passing language and runs on distributed memory parallel machines.

4 Results and Discussion

Flow conditions and flame conditions corresponding to the simulations appear on Table I. Two parameters have been varied, the heat release ratio T_p/T_f and the normalized turbulence intensity u'/S_L . Therefore, the simulations provide information on how the heat release and turbulence intensity affect the flow field and turbulent flame structure. Other important parameters such as S_L , U_o and l have been held constant, with the exception of R4.20.25, where $S_L=0.25\text{m/s}$. These parameters will be examined in future studies. The computational grid chosen was 220×300 with 128×128 points in the core grid region and 64 points were used to resolve the turbulent jet flow. This resolution is finer than that of our earlier study (Smith and Menon, 1997) in order to better resolve the flame wrinkling.

The mean jet velocity (U_o) was 5m/s and the integral length scale (l) was 0.0053 m (each l was resolved with approximately 6 grid cells). The "flame" G profile was resolved with 5 to 7 points making the effective $\delta_t \approx$ three to five mm (significantly higher than real flames). The integral scale increases in two-dimensional turbulence as it advances towards the wall so the flow resolution increases. However, the flame structure remains nearly constant in width and so the resolution of the flame remains nearly the same everywhere in the core region. The exception to this is when cusps arise which can be a concern using the G equation model with constant flame speed. Cusps create very high curvatures that can not be resolved. However, the present non-constant flame speed simulations combined with very energetic turbulence prevent cusps from becoming a problem.

Each simulation ran for at least a million time steps requiring about two thousand cpu hours using 64 nodes on a Cray T3E. This corresponds to roughly 95 large-eddy turnover times for flames R1.20, R4.20, and R7.20

and roughly 6.3 flow through times for all flames, where a flow through time is defined as $4D/U_o$. Statistics were generated from the final 80% of the data.

Figures 2a and 2b are snapshots of two flow simulations R7.5 and R7.20 highlighting the difference in these wrinkled flames with varying u'/S_L . Flame R7.5 is nearly planar and shows only small perturbations to the surface while flame R7.20 is highly convoluted, positioned further upstream away from the wall. It is also clear from the vorticity contours that more turbulence survives into the post flame region in flame R720. Figure 3 is taken from a video tape provided by Dr. R. K. Cheng. In these tomographic images the flow is from bottom to top, the light colored portion is reactants, the black, products. The flame structures are similar however it is clear that the experimental flames exhibit higher curvatures than do these simulations.

The Reynolds time averaged mean axial velocities for different simulations are shown in Figs. 4a-4c. In Fig. 4a, the turbulence intensity has been varied for a constant heat release of $T_p/T_f = 4$. Note that the velocity decreases non-linearly at the jet exit and reaches a linear decay only near the wall. This is due to the zero divergence at the jet nozzle. For low u'/S_L , the acceleration in velocity through the flame is distinct. As u'/S_L increases and the flame normal direction becomes more random this organized acceleration is reduced. The amount of heat release is varied for constant u'/S_L in Figs. 4b and 4c. The effect of increasing heat release is an increased acceleration through the flame and a mean flame positioned further from the wall. At higher intensity (Fig. 4c), the acceleration is again reduced compared to the lower intensity case. However, the flame position is even further away from the wall due to the increased burning rate.

The Reynolds time averaged r.m.s. axial velocity components are shown as a function of turbulence intensity holding the heat release constant in Figs. 5a-5c. Only a qualitative comparison with Cho *et al.* (1986) is shown since, the inflow intensity is not matched between the experiments and the simulations. The most important difference between these two-dimensional simulations and the axisymmetric experiments is the decay in turbulence intensity. Nevertheless, near-flame and post-flame characteristics are very similar. In all cases v' increases in the vicinity of the wall. It should be kept in mind that the wall boundary is a velocity slip condition, so v' does not decay to zero at the wall as it does in reality. In the low u'/S_L cases, u' increases through the flame.

In summary, the analysis of the time averaged velocity data, suggest that the effect of heat release on the flow is significant at low u'/S_L and diminishes as u'/S_L increases. The flame structure is examined next.

In the beginning of this section it was stated that the G structure was resolved over five to seven cells making these simulated flames much thicker than their experimental counter parts. As the two-dimensional turbulence evolves the small scales quickly dissipate resulting in larger length scales at the flame zone than at the jet exit. Flamelet combustion is implicitly assumed by our choice of flamelet approach. From Table I, the Damköhler numbers ($Da = (l/\delta_l)/(u'/S_L)$) based on the flame thickness, $\delta_l = \nu/S_L$, where ν is the reactant kinematic viscosity, are all greater than unity and the Karlovitz numbers ($Ka = (\delta_l/\eta)^2$) where $\eta = l/Re^{3/4}$ is the Kolmogorov length scale and $Re = u'l/\nu$, range from 0.18 to 1.42 for the $S_L = 0.5\text{m/s}$ flames. These Ka numbers are somewhat high but the small scales are increasing as the flow evolves. To test whether the flamelet assumption is valid the probability density function (pdf) of the progress variable defined as $C = 1 - G$ is plotted as a function of the mean progress variable $\langle C \rangle$ for the high intensity simulations in Fig. 6. In all the cases, the pdf is bimodal which means that within the turbulent flame zone the progress variable is overwhelming either unreacted or fully reacted. This result confirms that the flamelet assumption is valid for these conditions.

The turbulent flux that appears as an unclosed term in the Favre averaged species equation is an important term that accounts for the turbulent diffusion of reacting scalars and must be modeled. It is common to assume a gradient diffusion model

$$\overline{\rho u'' c''} = \overline{\rho u''} \overline{c''} = -\frac{\mu_t}{\sigma_c} \frac{\partial \overline{c}}{\partial x_i} \quad (8)$$

where μ_t is an eddy viscosity, σ_c is the turbulent Schmidt number and x_i is a Cartesian coordinate component. The presence of counter-gradient diffusion in turbulent premixed combustion has been well established in theory (Libby and Bray, 1981), experiments (Cho *et al.*, 1988; Li *et al.*, 1996) and in direct numerical simulation (DNS) (Veynante *et al.* 1995, 1997). The turbulent flux normalized by the reactant density (ρ_o) and the mean jet velocity (U_o) are shown in Figs. 7a-7d. The abscissa is normalized by the distance from the jet exit to the wall ($2D$). In Fig. 7a, the turbulence intensity is varied with no heat release. The turbulent flux is of gradient type (-) for all three cases increasing in magnitude as the intensity increases. In Fig. 7b $\overline{\rho u'' c''}$ changes from counter-gradient (+) (low u') to gradient (higher u') (-). Also note that the flame brush becomes broader with increasing u' . In Figs. 7c and 7d, the heat release is varied for the low u' flames and the high u' flames. The trends are the same. Gradient diffusion occurs in the no heat release cases and counter-gradient diffusion is observed for higher heat release. The high

u' flames are thicker than the low u' flames and the high heat release flames are pushed away from the wall.

Another way to look at the effect of heat release and u'/S_L on the turbulent flux is to plot it in progress variable space where all the flames are mapped to the average \tilde{C} . These are shown in Figs. 8a-8d. Of particular interest is Fig. 8d in which both gradient and counter-gradient diffusion exists in the high heat release, high u' flame (R7.20).

In Figs. 9a-9c, the flame surface densities (Σ) for different T_p/T_f are plotted at $u'/S_L = 1, 2, 4$ respectively. In two-dimensions, this is the flame length per unit area. It has a unit of 1/mm which is customary in the experimental literature. There are several ways to calculate this quantity (Trouvé *et al.* 1994; Peters 1997). The method chosen here is to define a small range in the progress variable. \tilde{C} is divided into a number of equal partitions. From the gradient $|\nabla C|$ at each location in the flame brush, if C is within the desired range $|\nabla C|$ is stored in the appropriate \tilde{C} partition and averaged. With the exception of some scatter towards the back of the flame ($\tilde{C} \approx 0.8$) for the no heat release cases, Σ tends to converge. This trend is observed in experiments of stagnation point flames.

The curvature distribution is compared to the experimental data of Shepherd and Ashurst (1992) in Fig. 10, with all of their flames at $u'/S_L < 1$. The pdf of flame curvature collapses when normalized by the r.m.s. curvature. The simulated flames show similar magnitude but differ significantly from the experimental flames. Flame R7.10 matches more closely in both u'/S_L and heat release than do the other two flames and it matches with the experimental flames reasonably well in shape but not magnitude.

The normalized turbulent flame speed u_t/S_L , is plotted as a function of u'/S_L in Fig. 11. The turbulent flame speed is defined as the value of $\langle U \rangle$ where the slope begins to change (Cho *et al.* 1986; Liu and Lenze, 1988). For no heat release cases, The value of $\langle U \rangle$ is chosen where $\langle C \rangle$ obtains a value of 0.02. This value was determined from averaging $\langle C \rangle$ for the heat release cases once the location had been determined from where the slope changed. These two-dimensional simulations compare well with the data from Cho *et al.* (1986) but under predict the data of Liu and Lenze, (1988) significantly.

4.1 LES-LEM Flame Propagation

To the best of the authors' knowledge, this work represents the first attempted premixed unsteady reacting simulations of stagnation point flames. Though mostly qualitative in nature, the agreement with experimental data is quite encouraging. Simulations like these can

provide a database for the evaluation of other models such as the LES-LEM model which has a range of applicability exceeding the flamelet regime.

The LEM is calibrated using a stand alone model of flame propagation into isotropic turbulence (Smith and Menon 1996). One calibration constant adjusts the stirring frequency to match the burning rates observed in stagnation point flame experiments. This calibration constant is then used in the subgrid model. The calibration curves are shown in Fig. 12.

Figures 13a and 13b show the effect of artificial flame reduction on propagation of a laminar flame. The flame is being convected to the right while burning into the fuel on the left. Without the flame reduction algorithm, the flame shape becomes distorted.

Figure 14 shows a snapshot vorticity contours and the filtered subgrid G field. The resolution is 25% less than the conventional G simulations and the $u'/S_L = 8$, $Re=200$ and $T_p/T_f = 4$. The flame structure looks similar to Fig. 2b though scales of wrinkling are noticeably smaller resulting in less resolved flame area. The smaller flame area is compensated for by the subgrid wrinkling.

To study the propagation mechanisms in the LES-LEM approach, three propagation speeds are defined. Collection of data only includes the core region which is defined as the twice the width of the forced jet. The first is A_{LES}/A_L , the resolved scale area ratio. For this geometry, A_L is simply the width of the domain (which is the twice the width of the forced jet). In flamelet combustion, the area ratio is approximately the ratio of the turbulent to laminar flame speed. The second propagation speed defined as the subgrid turbulent flame speed (u_{tsgs}/S_L) is a global average of the ratio of the number of flame crossings to a single (laminar) flame crossing. The global average is taken over all LES cells containing at least one flame crossing within the core region. The third propagation speed is the global scalar consumption rate. It is defined as ($S_G = \frac{\Delta x_{LEM}}{\Delta t_{sgs}} \sum_{i=1}^{JMAX} \sum_{j=1}^{JMAX} \Delta G$, where Δx_{LEM} is the subgrid cell spacing and Δt_{sgs} is the subgrid integration time step size). S_G represents the global destruction of G . In Fig. 15a-15c the three propagation rates are shown for the LES-LEM with $T_p/T_f = 4$. The time axis is normalized by the large-eddy turnover time. In fig. 15a, A_{LES}/A_L achieves a nearly stationary value of two for all three cases. This is characteristic of the filtered LEM field where instead of resolving most of the flame area, a significant portion of the flame area is in the subgrid. The average subgrid burning rate (Fig. 15b) shows how the flame burning rate responds to increased u'/S_L the creation/destruction of flame crossings due to stirring and normal propagation. Figure 15c is a global average of the burning rate due to a

combination of resolved flame area and subgrid burning rates. Again, it scales properly with u'/S_L so that even though the resolved area is not very different for these three flames, the effect of the subgrid burning dominates in the overall burning rate yielding the correct scaling with u'/S_L .

5 Conclusions

A methodology for simulating turbulent premixed flame propagation in the flamelet regime has been developed and applied to stagnation point flows. Extensions to earlier work (Smith and Menon, 1997) have been carried out. Two combustion models are studied, the G equation and the LES-LEM. The key issues involving the conventional flamelet model have to do with subgrid closure and whether or not the gradient diffusion assumption is valid even in the subgrid. The heat release and normalized turbulence intensity were varied and the effects on the flow field and flame structure were studied. The major results seem to suggest that the heat release plays a dominant role in determining the flow field and flame structure at low u'/S_L but plays a diminishing role as u'/S_L increases. Results presented in the form of time averaged statistics show significant counter-gradient diffusion of the turbulent scalar flux even though a gradient based model is used. However, these two-dimensional simulations may not include significant levels of unresolved energy and therefore these results may require three-dimensional tests in order to resolve this issue.

Further development of the LES-LEM model is also reported. In particular, thermodynamic coupling between the subgrid combustion and the resolved LES field, and a new splicing algorithm that eliminates spurious diffusion has been developed. Detailed studies of turbulent stagnation point flames using the new LES-LEM model are planned. The front tracking algorithm which includes splicing, artificial flame reduction and inter-LES cell burning plays a key role in the overall performance of the LES-LEM simulations. Qualitative trends in the burning rates with varying turbulence intensity have been demonstrated.

Acknowledgments

This work was supported in part by the Air Force Office of Scientific Research under the Focused Research Initiative, monitored by General Electric Aircraft Engines, Cincinnati, Ohio. Support for the computations was provided by the Navo HPC and the Pittsburgh Super Computing Center through NSF and is gratefully acknowledged.

References

- Bray, K. N. C. (1995) "Turbulent Transport in Flames," *Proc. R. Soc. Lond. A*, Vol. 451, pp. 231-256.
- Calhoon, W. H. and Menon, S. (1997) "Linear-Eddy Subgrid Model for Reacting Large-Eddy Simulations: Heat Release Effects," Presented at the 35th Aerospace Sciences Meeting, Reno, Nv, January 6-9 AIAA-97-0368.
- Calhoon, W. H. and Menon, S. (1996) "Subgrid Modeling for Reacting Large Eddy Simulations," Presented at the 34th Aerospace Sciences Meeting, Reno, Nv, January 15-18 AIAA-96-0516.
- Cho, P., Law, C. K., Cheng, R. K., and Shepherd, I. G. (1988) "Velocity and Scalar Fields of Turbulent Premixed Flames in Stagnation Flow," *Twenty-Second Symposium (International) on Combustion*, The Combustion Institute, Pittsburgh, pp. 739-745.
- Cho, P., Law, C. K., Hertzberg, J. R., and Cheng, R. K. (1986) "Structure and Propagation of Turbulent Premixed Flames Stabilized in a Stagnation Flow," *Twenty-first Symposium (International) on Combustion*, The Combustion Institute, Pittsburgh, pp. 1493-1499.
- Ferziger, J. H. (1983) "Higher-Level Simulations of Turbulent Flows," in *Computational Methods for Turbulent, Transonic and Viscous Flows*, Hemisphere Publishing Company.
- Im, H. G. (1995) "Study of turbulent premixed flame propagation using a laminar flamelet model," *Center For Turbulent Research, Annual Research Briefs*, pp. 347-360.
- Im, H. G. Lund, T. S. and Ferziger, J. H. (1997) "Large Eddy Simulation of Turbulent Front Propagation With Dynamic Subgrid Models," *Phys. of Fluids*, Vol. 9, no. 12., pp. 3826-3833.
- Kerstein, A. R. (1991) "Linear-Eddy Modeling of Turbulent Transport. Part 6. Microstructure of Diffusive Scalar Mixing Fields," *J. Fluid Mech.*, Vol. 231, pp. 361-394.
- Lee, S., Lele, S. K., and Moin, P. (1992) "Simulation of spatially evolving turbulence and the applicability of Taylor's Hypothesis in compressible flow," *Phys. of Fluids A*, Vol. 4, pp. 1521-1530.

- Li, S. C., Libby, P. A. and Williams, F. A. (1994) "Experimental Investigation of a Premixed Flame in an Impinging Turbulent Stream," *Twenty-fifth Symposium (International) on Combustion*, The Combustion Institute, Pittsburgh, pp. 1207-1214.
- Libby, P. A. and Bray, K. N. C. (1981) "Countergradient Diffusion in Premixed Turbulent Flames" *AIAA Journal*, Vol. 19, No. 2.
- Liu, Y., and Lenze, B. (1988) "The Influence of Turbulence on the Burning Velocity of Premixed $CH_4 - H_2$ Flames with Different Laminar Burning Velocities," *Twenty-Second Symposium (International) on Combustion*, The Combustion Institute, Pittsburgh, pp. 747-754.
- Menon, S. (1991) "Active Control of Combustion Instability in a Ramjet Using Large-Eddy Simulations," AIAA-91-0411, 29th Aerospace Sciences Meeting, Reno, Nv, January 7-10.
- Menon, S., and Jou, W.-H. (1991) Large-Eddy Simulations of Combustion Instability in an Axisymmetric Ramjet Combustor, *Combust. Sci. and Tech.*, Vol. 75, pp. 53-72.
- Menon, S. and Kerstein, A. R. (1992) "Stochastic Simulation of the Structure and Propagation Rate of Turbulent Premixed Flames," *Twenty-Fourth Symposium (International) on Combustion*, The Combustion Institute, Pittsburgh, pp. 443-450.
- Menon, S., McMurtry, P. A. and Kerstein, A. R. (1994) "A Linear Eddy Subgrid Model for Turbulent Combustion: Application to Premixed Combustion," Presented at the 31st Aerospace Sciences Meeting, Reno, Nv, January 11-14, AIAA-94-0107.
- Nelson, C. C. and Menon, S. (1998) "Unsteady Simulations of Compressible Spatial Mixing Layers," AIAA 98-0786 Presented at the 36th AIAA Aerospace Sciences Meeting and Exhibit, January 12-15, Reno Hilton, Reno, NV.
- Peters, N. (1997) The Turbulent Burning Velocity for Large Scale and Small Scale Turbulence," *To be submitted to J. Fluid Mech.*
- Piana, J., Durcros, F., and Veynante, D. (1997) "Large Eddy Simulations of Turbulent Premixed Flames Bases on the G-Equation and a Flame Front Wrinkling Description," *11th Symposium on Turbulent Shear Flows*, Grenoble France.
- Poinsot, T, J., and Lele, S. K. (1992) "Boundary Conditions for Direct Simulation of Compressible Viscous Flows," *J. Comp. Phys.*, Vol. 101 pp. 104-129.
- Shepherd, I. G. and Ashurst, Wm. T. (1992) "Flame Front Geometry in Premixed Turbulent Flames," presented at the *Twenty-Fourth Symposium (International) on Combustion*, The Combustion Institute, Pittsburgh, pp. 485-491.
- Smith, T. and Menon, S. (1997) "Large-Eddy Simulations of Turbulent Reacting Stagnation Point Flows," AIAA-97-0372, Reno, NV, January 6-10.
- Smith, T. and Menon, S. (1996a) "Model Simulations of Freely Propagating Turbulent Premixed Flames," presented at the *Twenty-sixth Symposium (International) on Combustion*, The Combustion Institute, Pittsburgh, pp. 299-306.
- Smith, T. and Menon, S. (1996b) "One-Dimensional Simulations of Freely Propagating Turbulent Premixed Flames," *Accepted for publication in Combust. Sci. Tech.*, April.
- Trouvé, A. and Poinsot, T. (1994) "The Evolution Equation for the Flame Surface Density in Turbulent Premixed Combustion," *J. Fluid Mech.*, Vol. 278, pp. 1-31.
- Veynante, D., Trouvé, A., Bray, K. N. C., and Mantel, T. (1997) "Gradient and Counter-Gradient Scalar Transport in Turbulent Premixed Flames," *J. Fluid Mech.*, Vol. 332., pp. 263-293.
- Veynante, D., and Poinsot, T. (1995) "Effects of Pressure Gradients on Turbulent Premixed Flames," *Center for Turbulence Research, Annual Research Briefs*, pp. 273-300.
- Williams, F. A. (1985) "Turbulent Combustion," *In The Mathematics of Combustion*, Ed. Buckmaster, J. D., Society for Industrial and Applied Mathematics, pp 97-131.
- Yakhot, V. (1988) Propagation Velocity of Premixed Turbulent Flames, *Combust. Sci. Tech.*, 60, pp. 191-214.

Table I. Turbulent Flame Properties.

Run	Rel	Da	U m/s	S_L m/s	T_p/T_f	u'/S_L	u_t/S_L
R1.5	32	32	5	0.5	1	0.313	2.44
R1.10	63	16	5	0.5	1	0.987	3.38
R1.20	127	8	5	0.5	1	2.45	5.87
R4.5	32	32	5	0.5	4	0.257	1.58
R4.10	63	16	5	0.5	4	1.08	3.72
R4.20	127	8	5	0.5	4	2.47	4.70
R4.20.25	127	4	5	0.25	4	5.27	10.9
R7.5	32	32	5	0.5	7	0.313	1.85
R7.10	63	16	5	0.5	7	0.719	2.38
R7.20	127	8	5	0.5	7	2.90	5.20

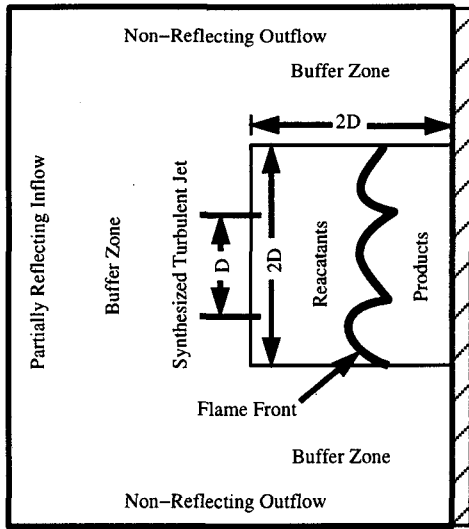


Figure 1. Schematic of stagnation point flame Simulations.

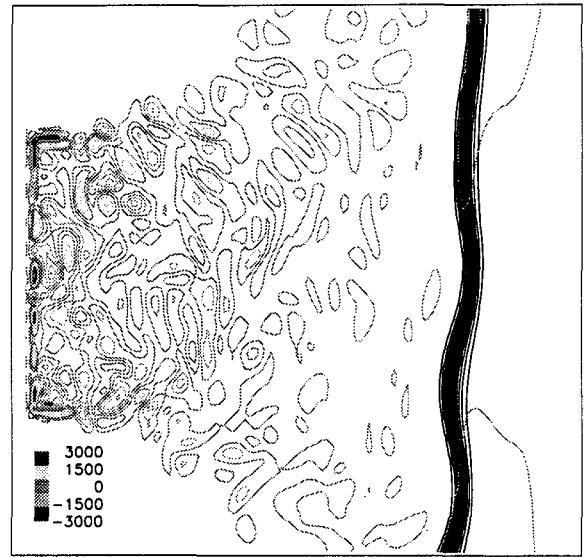


Figure 2a. Snapshot of vorticity contours and flame contours for flame R7.5.

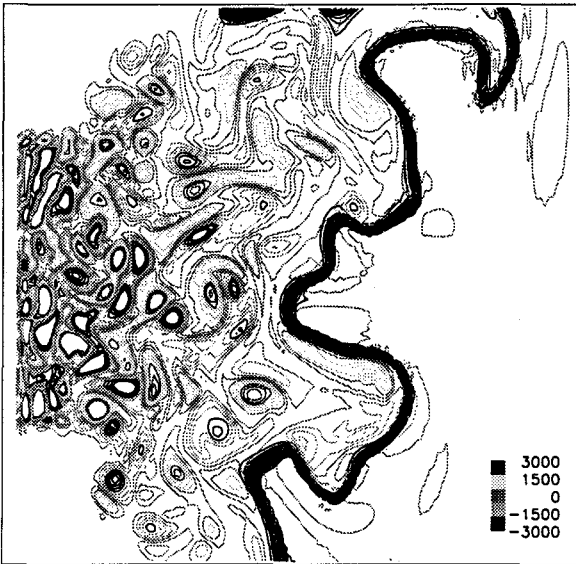


Figure 2b. Snapshot of vorticity contours and flame contours for flame R7.20.

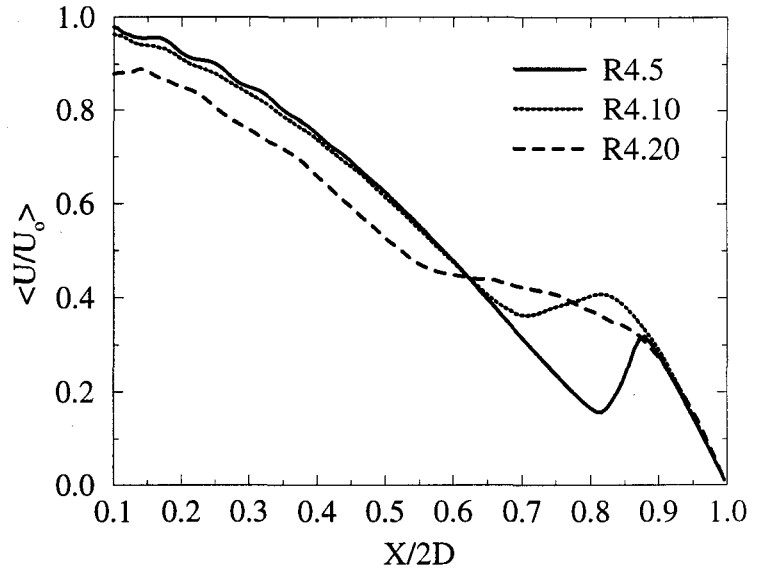


Figure 4a. Reynolds averaged axial velocity for different u'/S_L and $T_p/T_f=4$.

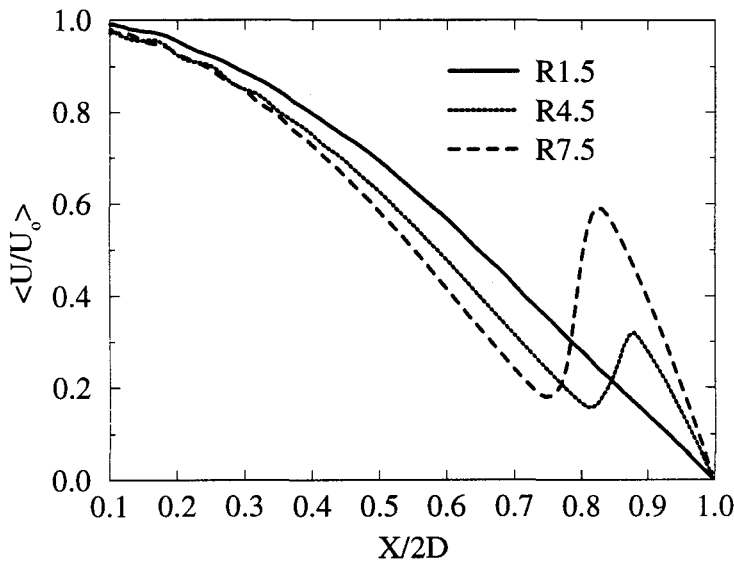


Figure 4b. Reynolds averaged axial velocity for different T_p/T_f and $u'/S_L=1$.

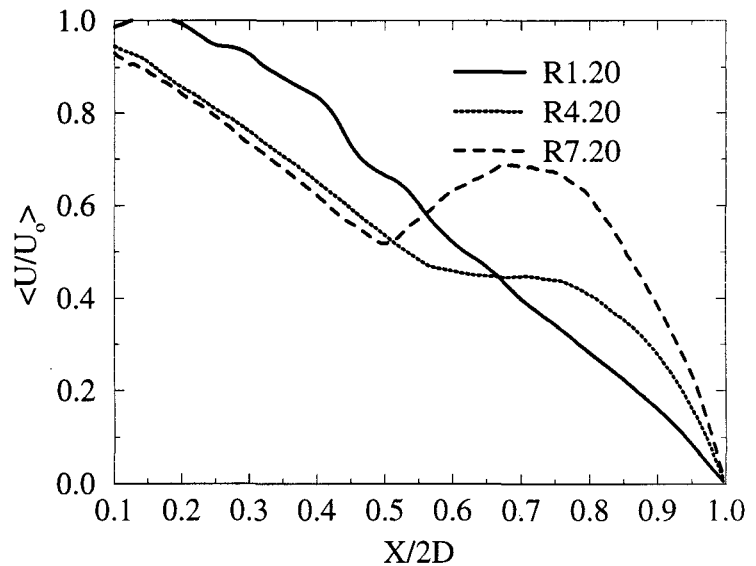


Figure 4c. Reynolds averaged axial velocity for different T_p/T_f and $u'/S_L=4$.

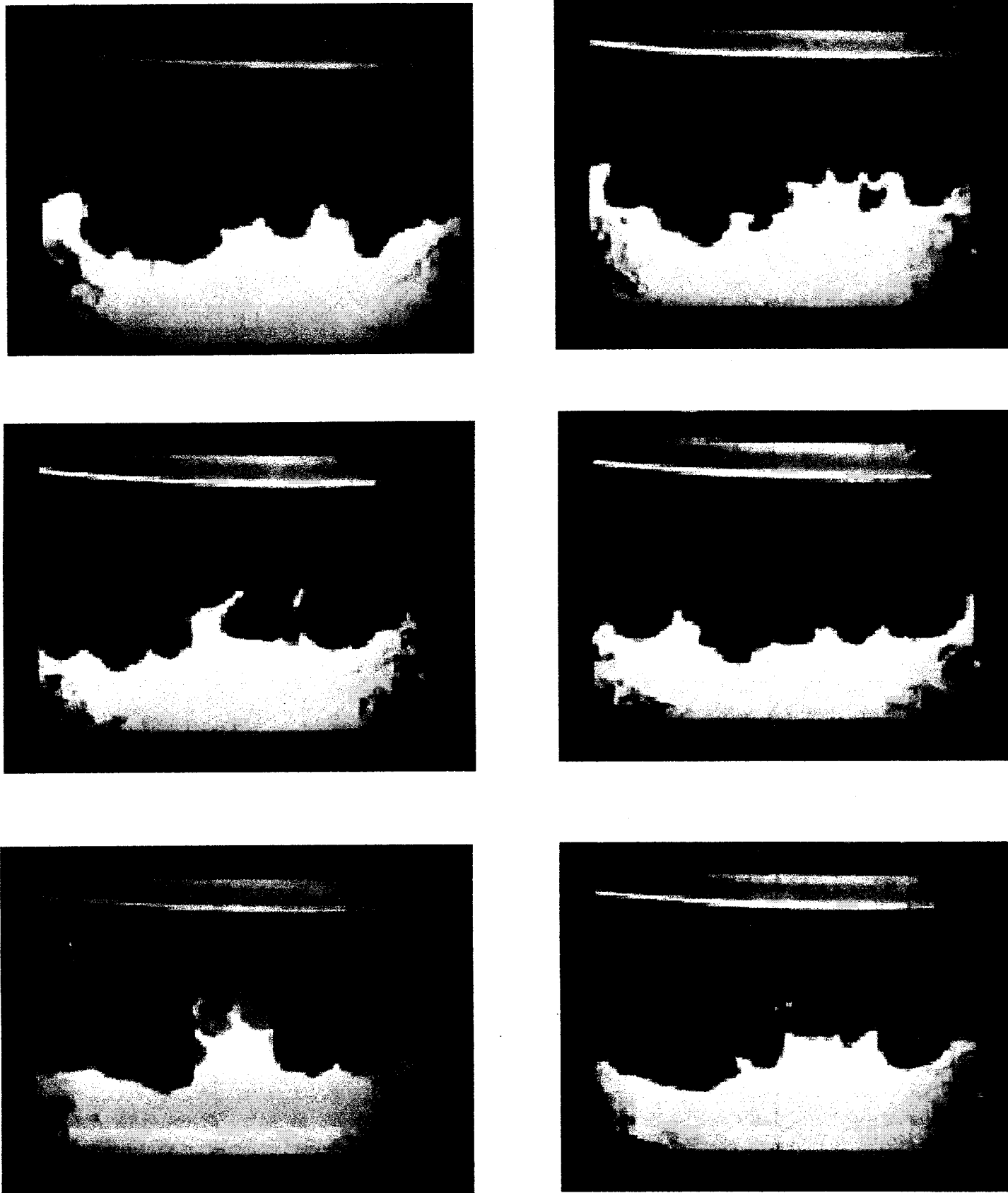


Figure 3. Tomographic images courtesy of R. K. Cheng, LBNL.

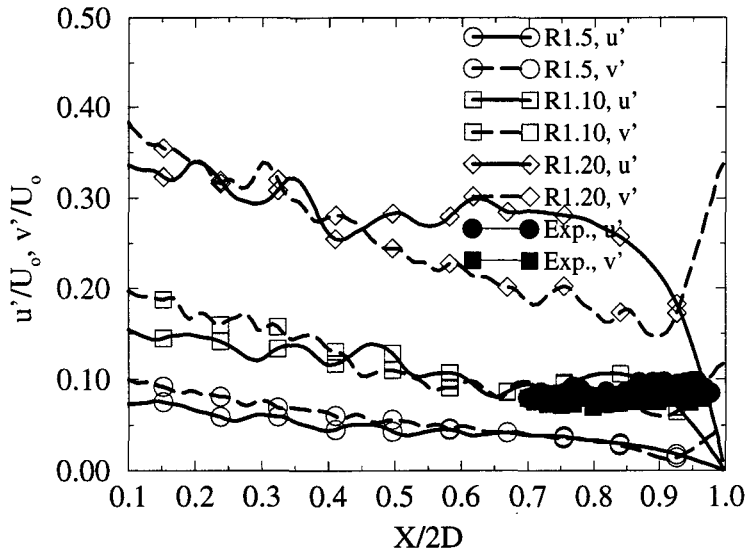


Figure 5a. Reynolds averaged r.m.s. components of velocity for different u'/S_L and $T_p/T_f=1$.

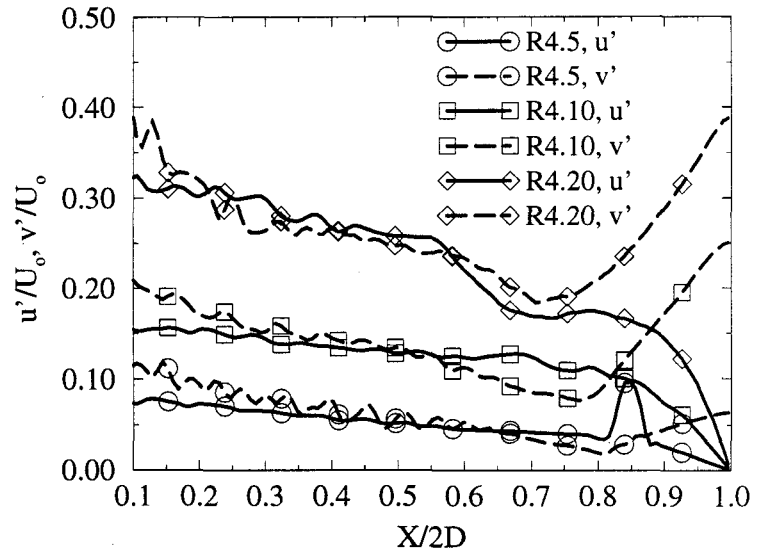


Figure 5b. Reynolds averaged r.m.s. components of velocity for different u'/S_L and $T_p/T_f=4$.

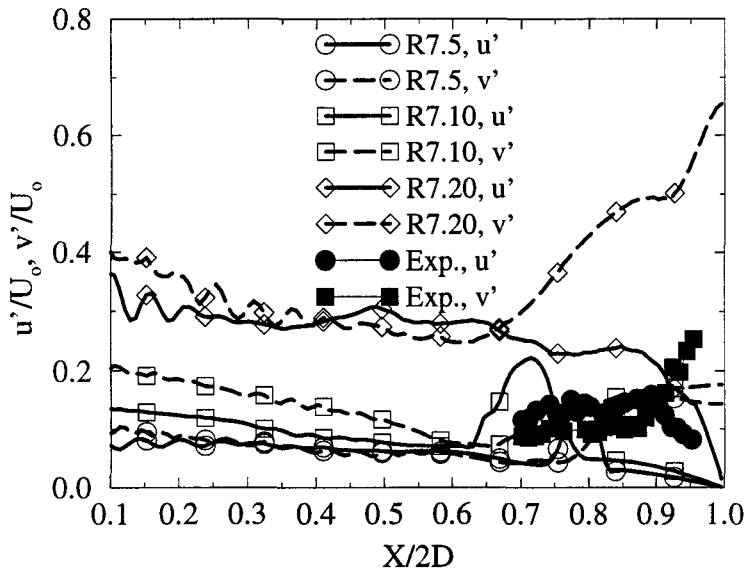


Figure 5c. Reynolds averaged r.m.s. components of velocity for different u'/S_L and $T_p/T_f=7$.

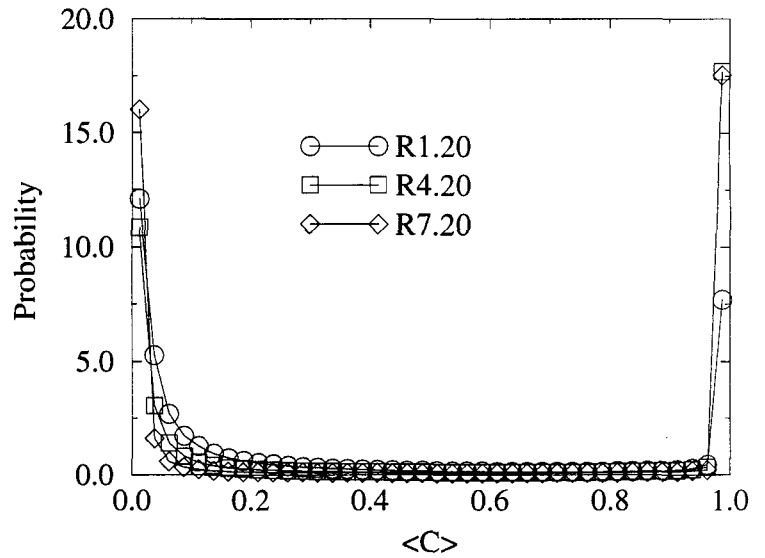


Figure 6. Probability density function for the progress variable.

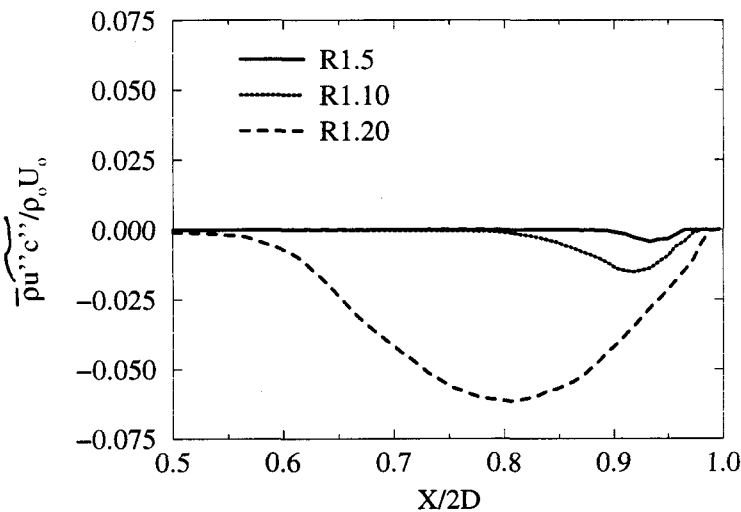


Figure 7a. Turbulent flux as a function of axial location for different u'/S_L and $T_p/T_f=1$.

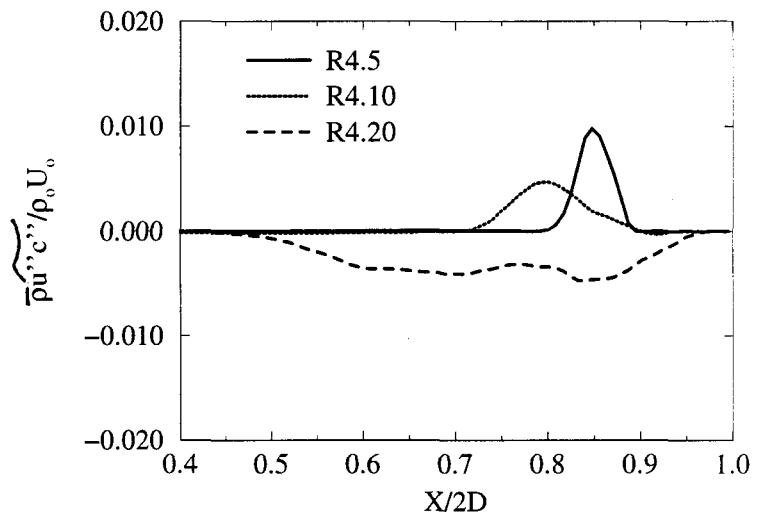


Figure 7b. Turbulent flux as a function of axial location for different u'/S_L and $T_p/T_f=4$.

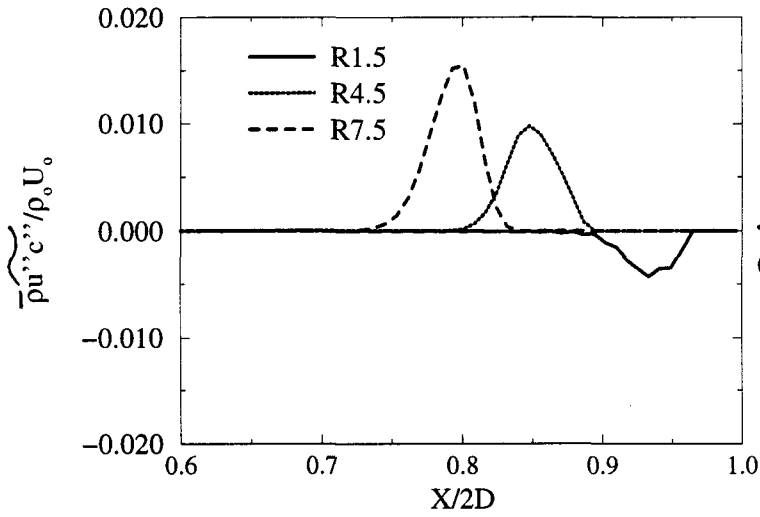


Figure 7c. Turbulent flux as a function of axial location for different T_p/T_f and $u'/S_L=1$.

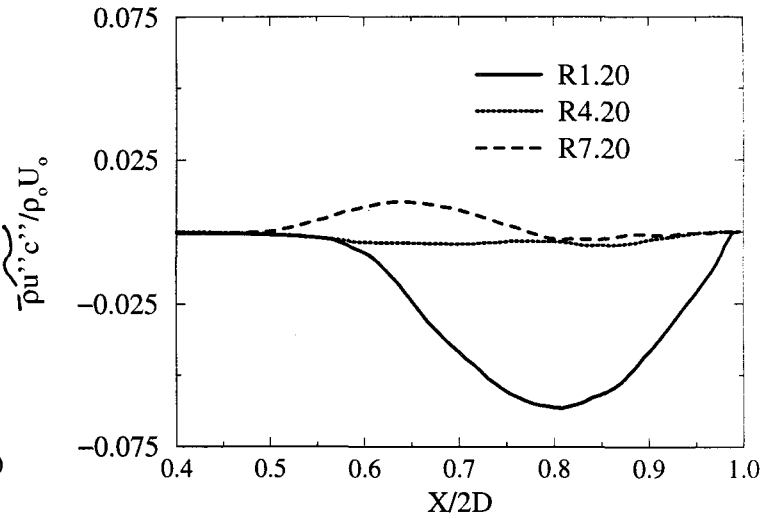


Figure 7d. Turbulent flux as a function of axial location for different T_p/T_f and $u'/S_L=4$.

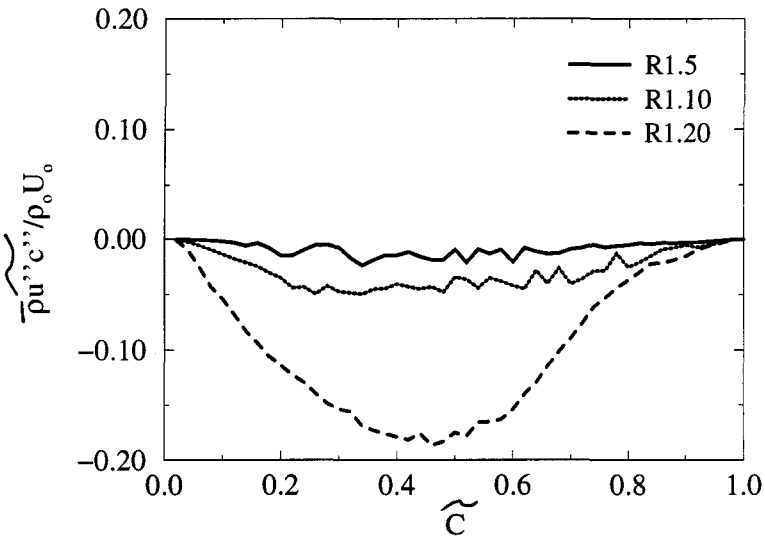


Figure 8a. Turbulent flux as a function of progress variable for different u'/S_L and $T_p/T_f=1$.

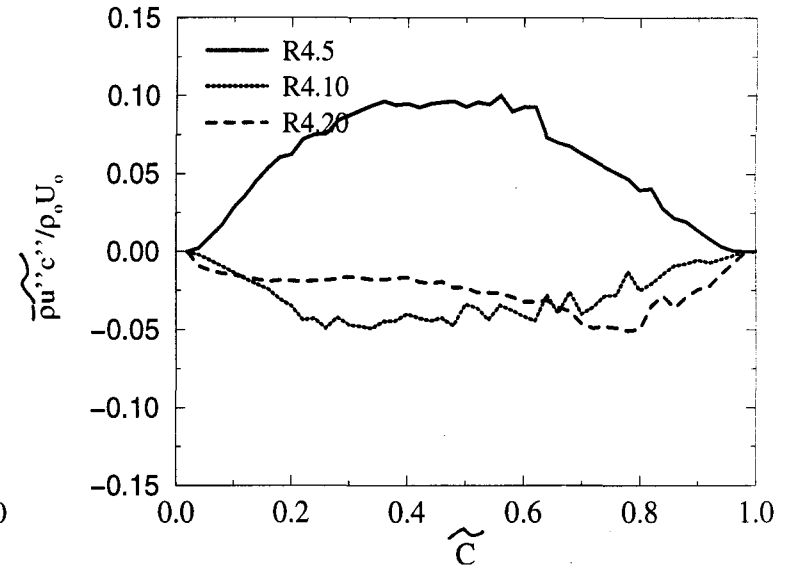


Figure 8b. Turbulent flux as a function of progress variable for different u'/S_L and $T_p/T_f=4$.

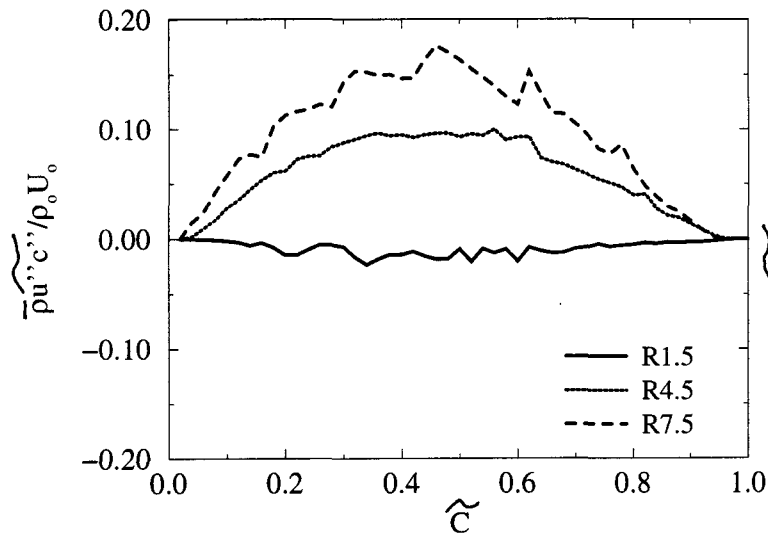


Figure 8c. Turbulent flux as a function of progress variable for different T_p/T_f and $u'/S_L=1$.

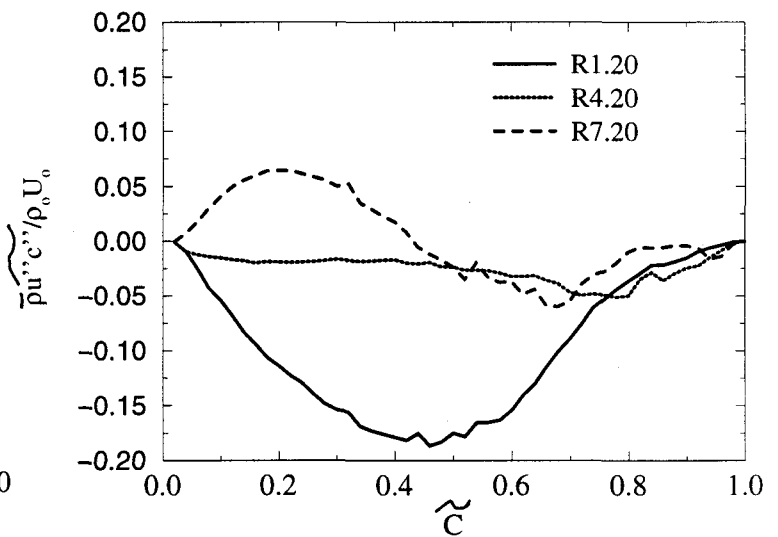


Figure 8d. Turbulent flux as a function of progress variable for different T_p/T_f and $u'/S_L=4$.

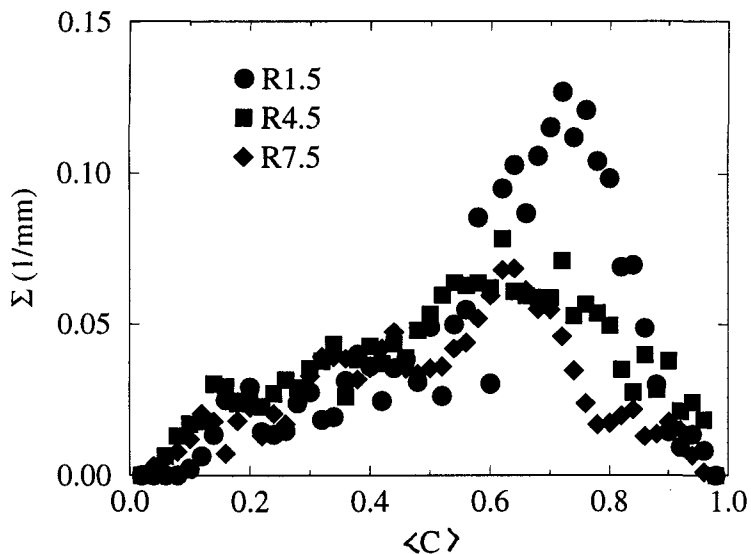


Figure 9a. Flame surface density as a function of progress variable for different T_p/T_f and $u'/S_L=1$.

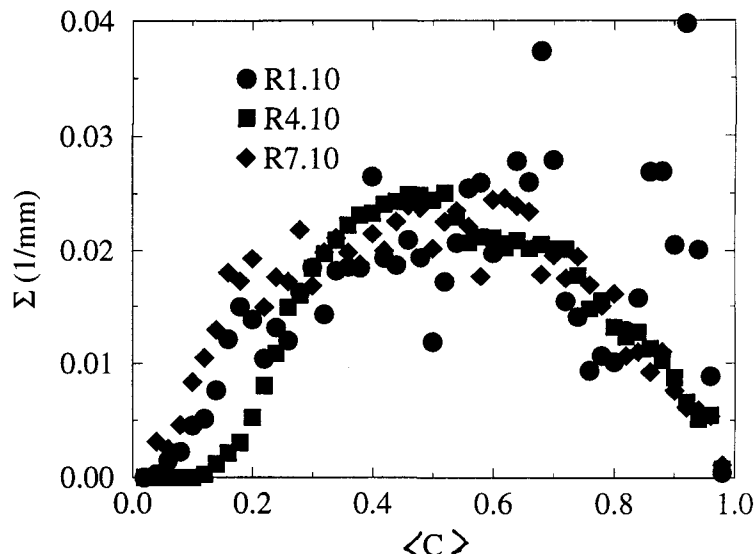


Figure 9b. Flame surface density as a function of progress variable for different T_p/T_f and $u'/S_L=2$.

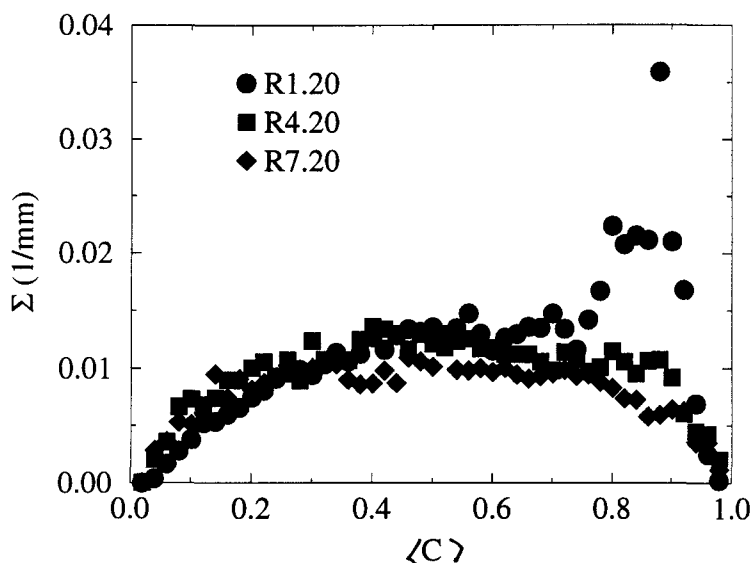


Figure 9c. Flame surface density as a function of progress variable for different T_p/T_f and $u'/S_L=4$.

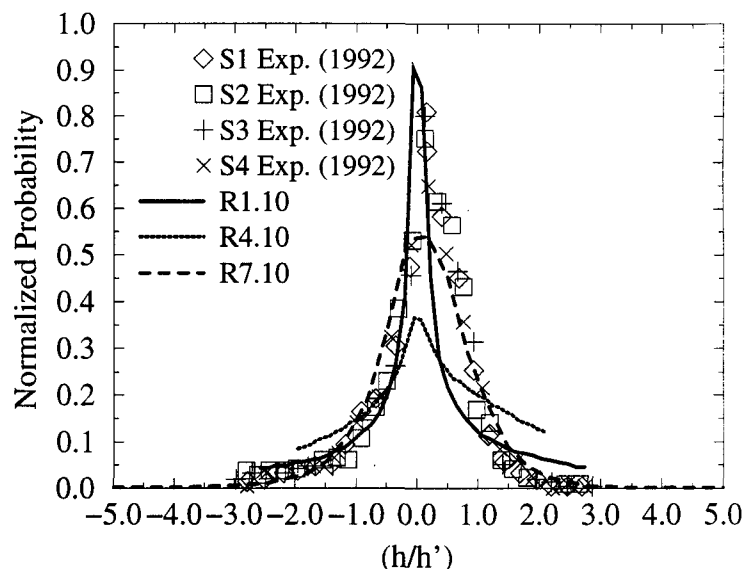


Figure 10. Normalized probability density of curvature.

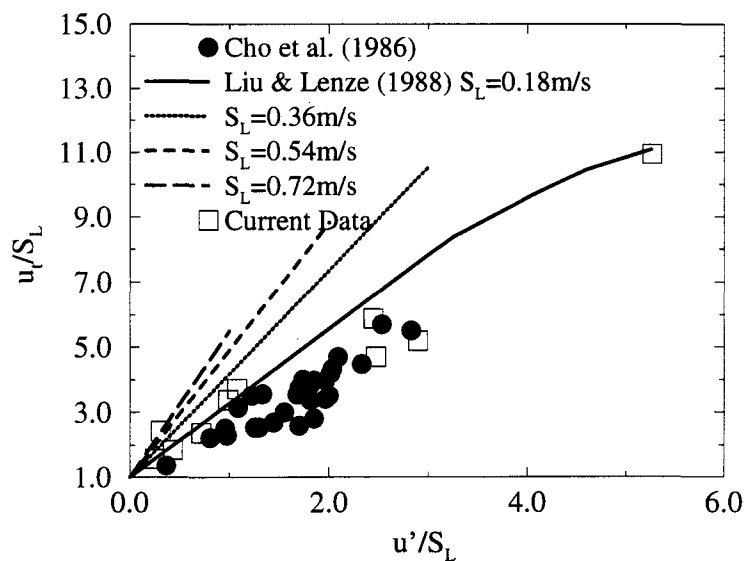


Figure 11. Turbulent flame speed.

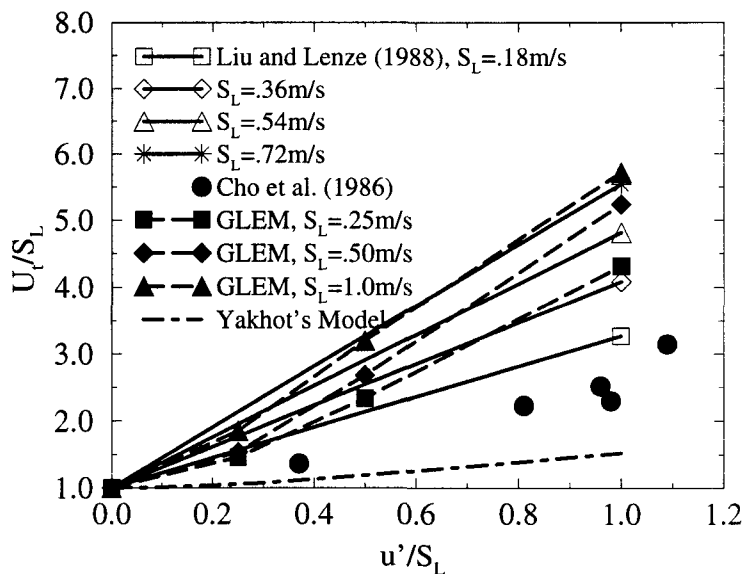


Figure 12. LEM subgrid calibration.

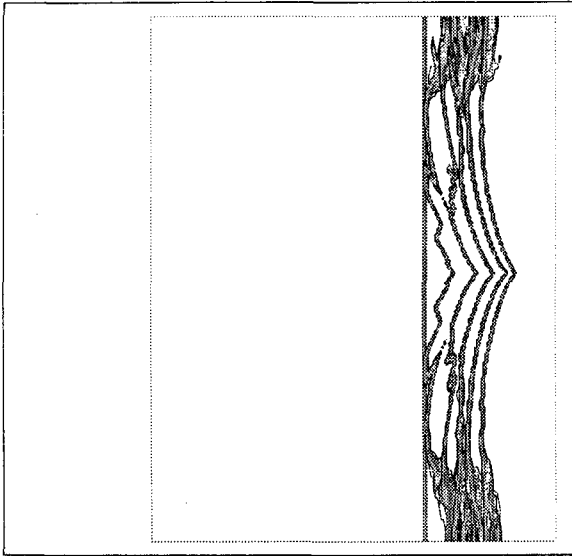


Figure 13a. LEM Convection test without artificial flame reduction.

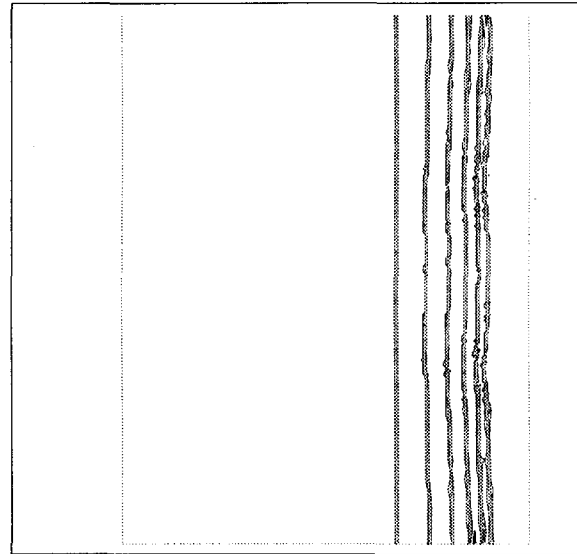


Figure 13b. LEM Convection test with artificial flame reduction.

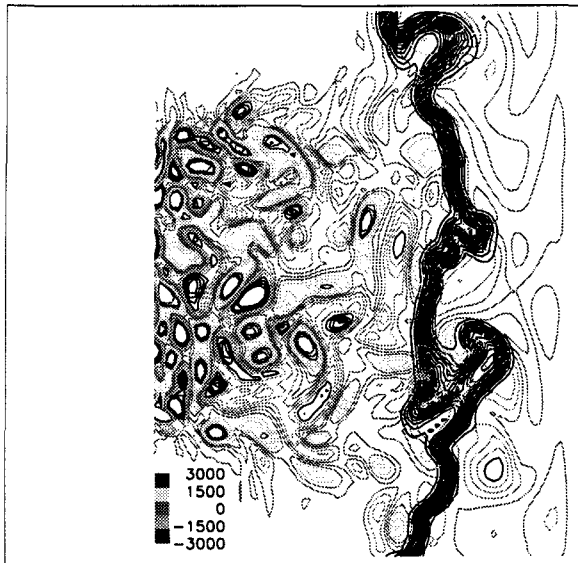


Figure 14. Snapshot of vorticity contours and filtered G field for LES-LEM.

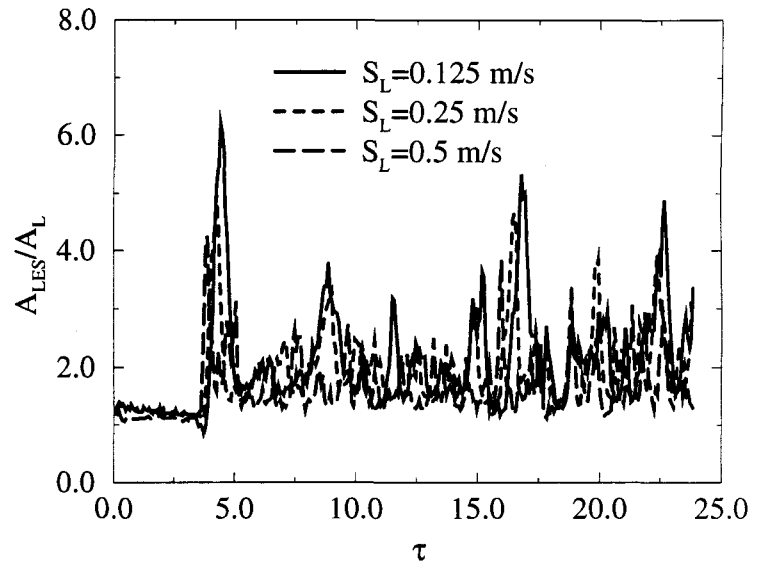


Figure 15a. Resolved Flame area.

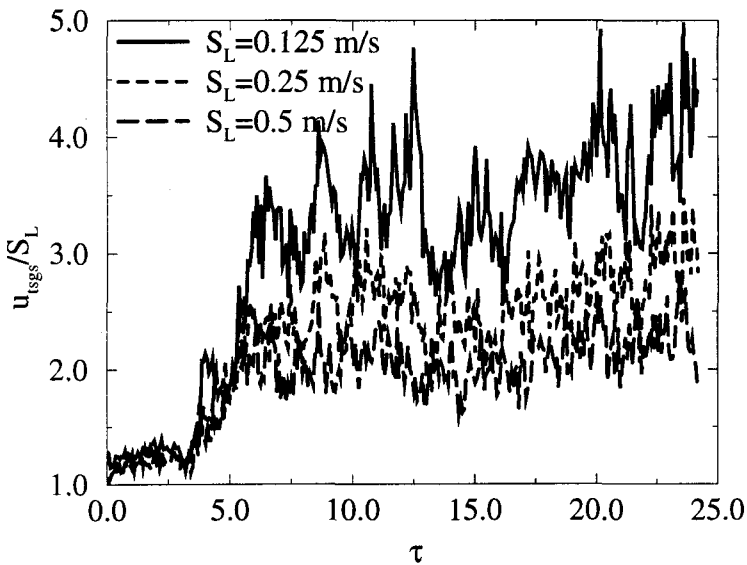


Figure 15b. Average subgrid burning velocity.

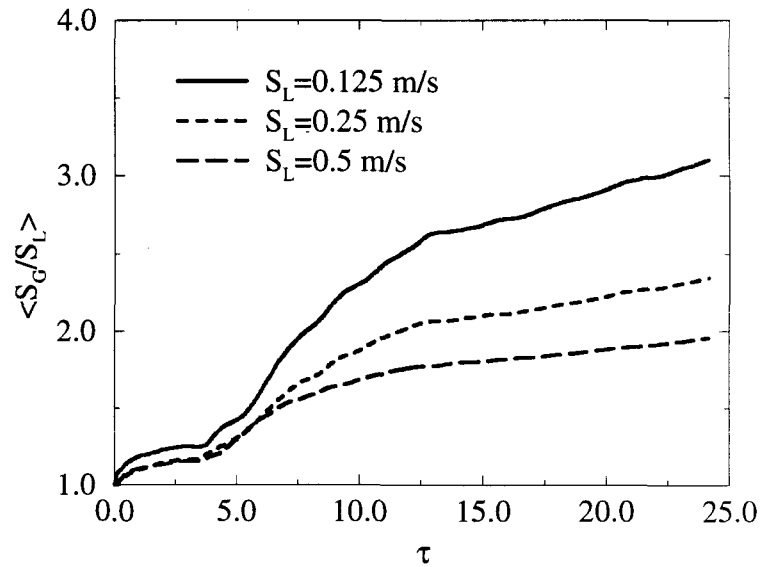


Figure 15c. Global propagation rate.